Journal of Magnetic Resonance 204 (2010) 228–238

Contents lists available at ScienceDirect

Journal of Magnetic Resonance

journal homepage: www.elsevier.com/locate/jmr

Experimental investigation and numerical simulation of ^{3}He gas diffusion in simple geometries: Implications for analytical models of ^{3}He MR lung morphometry

J. Parra-Robles *, S. Ajraoui, M.H. Deppe, S.R. Parnell, J.M. Wild *

Academic Unit of Radiology, University of Sheffield, UK

ARTICLE INFO

Article history:
Received 29 September 2009
Revised 22 February 2010
Available online 1 March 2010

Keywords:
Hyperpolarized helium
Lung diffusion
Cylinder model
Diffusion theory
Finite element simulations

ABSTRACT

Models of lung acinar geometry have been proposed to analytically describe the diffusion of ^{3}He in the lung (as measured with pulsed gradient spin echo (PGSE) methods) as a possible means of characterizing lung microstructure from measurement of the ^{3}He ADC. In this work, major limitations in these analytical models are highlighted in simple diffusion weighted experiments with ^{3}He in cylindrical models of known geometry. The findings are substantiated with numerical simulations based on the same geometry using finite difference representation of the Bloch–Torrey equation. The validity of the existing "cylinder model" is discussed in terms of the physical diffusion regimes experienced and the basic reliance of the cylinder model and other ADC-based approaches on a Gaussian diffusion behaviour is highlighted. The results presented here demonstrate that physical assumptions of the cylinder model are not valid for large diffusion gradient strengths (above ~15 mT/m), which are commonly used for ^{3}He ADC measurements in human lungs.

1. Introduction

Hyperpolarized noble gas MRI can provide information related to structural and physiological properties of lungs and has sensitivity to aspects of lung disease [1,2]. In particular, the measurement of the apparent diffusion coefficient, ADC (as measured with pulsed gradient spin echo (PGSE) methods), has been proven to be sensitive to the micro-structural changes in the lung caused by emphysema [3–8]. Relating the measured diffusion parameters to lung properties (e.g. airway diameter, surface area and connectivity) is a complicated task due to the non-Gaussian nature of gas diffusion in the lung [7,9], which results in a non-monoexponential behaviour of the diffusion-weighted MR signal. The non-monoexponential signal behaviour originates from a number of sources, including the anisotropic diffusion in airways, the presence of a range of airway dimensions and the branching structure of the lung [10]. Furthermore, the timing and strength of the diffusion weighting gradients is implicitly related to the confining length scale and gas diffusivity in defining the measured ADC [11]. As such, the concept of a ^{3}He ADC is of limited physical meaning as it assumes monoexponential signal behaviour and is thus underpinned by an assumption of Gaussian diffusion [12].

This problem is similar to that encountered in NMR diffusion investigations of porous materials, and much of the theory and experimental methods of MR diffusion has been developed previously in this context [13–15]. The correct application of this theory, particularly the concept of the localized diffusion regime (discussed later), has yet to be fully realized by the ^{3}He lung MRI community.

An analytical model ("cylinder model") has been proposed [7] that reduces the acinar structure to a large number of long non-connected cylinders which are uniformly oriented in all possible spatial directions. The formalism, originally developed by Callaghan et al. [14,16], was used to estimate two diffusion coefficients (D_L and D_T, which are defined in Section 2.2). Inherent to the treatment is the assumption of Gaussian diffusion in each cylinder as the non-monoexponential decay of the signal is attributed to originate from the superposition of the monoexponential signals of the individual cylinders. The Gaussian approximation was also used to obtain a relationship between the airway radius and the measured D_T values.

More elaborate expressions to describe the dependence of D_L and D_T on the geometrical parameters of a more complex model of alveolar ducts [17] (which incorporates alveolar septa to the cylinders) were recently obtained from Monte Carlo computer simulations [18]. In these expressions, the diffusion coefficients are made dependent upon the *b*-values to account for non-Gaussian signal behaviour in single airways. However, this "updated cylinder model" still relies on the expressions of the original cylinder model [7] (and hence on the validity of the Gaussian approximation), in order to estimate D_L and D_T from a fit to the signal decay.

* Corresponding authors. Address: Academic Unit of Radiology, Floor C, Royal Hallamshire Hospital, Glossop Road, Sheffield S10 2JF, UK.
E-mail addresses: J.Parra-Robles@sheffield.ac.uk (J. Parra-Robles), j.m.wild@sheffield.ac.uk (J.M. Wild).

1090-7807/$ - see front matter © 2010 Elsevier Inc. All rights reserved.
doi:10.1016/j.jmr.2010.02.023

There therefore exists some inconsistency in the theoretical basis of these detailed analytical models; moreover experimental validation has only been done indirectly by comparison to known average dimensions of lung airways [7,9]. In vivo experiments showed that the cylinder model produced reasonable estimates of the average airway diameters and that the estimated diffusion parameters (most significantly D_L) were sensitive to emphysema [7].

An alternative numerical approach has been proposed by Fichele et al., where computer simulations of ^{3}He diffusion were conducted by using finite difference treatment of the Bloch–Torrey equation [11,19] within different 2D and 3D geometries for different PGSE diffusion gradient weightings. All sources of non-Gaussian diffusion are intrinsically taken into account in this finite difference treatment. These simulations showed reasonable agreement with the cylinder model in the range of gradient strengths studied with the geometrical models generated, however, they did highlight that the cylinder model tends to overestimate the airway radius, but a physical explanation of this discrepancy was not attempted.

No investigation of the limits of validity of the most basic underlying physical assumption of the cylinder model (i.e. Gaussian phase approximation) or experimental validation of the cylinder model in well defined physical models (e.g. cylindrical phantoms) has yet been reported in the published ^{3}He lung MR literature. A phantom consisting of a single cylindrical loop was used by Emami et al. [20] to study anisotropic ^{3}He diffusion in experiments and Monte Carlo computer simulations, but no comparison of their results to the cylinder model nor analytical description of the diffusion signal were presented.

Evidence of the shortcomings of approaches based on the Gaussian approximation in explaining the results of ^{3}He MR diffusion experiments in lungs exists in the published literature. In vivo investigation of the role of gradient strength and diffusion time in ADC measurements has been reported [11] in lungs of healthy and smoker volunteers. The higher ADC values obtained for stronger gradients cannot be explained within the Gaussian diffusion approximation. Habib et al. [21] built a scale model of the Kitaoka labyrinth [22] that had been previously used in computer simulations of diffusion in acinar airways [22,23]. They found that in some cases a model of localized diffusion produced a better fit of the experimental data than a single exponential and the cylinder model [24]. However, no relationship between estimated diffusion parameters and structural sizes was inferred.

In this work, the basic assumptions of the models used to explain the ADC data obtained in ^{3}He gas MR diffusion experiments (in particular, the cylinder model) are tested experimentally in simple geometric models. The experimental designs developed for these tests, including phantom construction and new theoretical treatment, are presented. Finite element numerical simulations of the Bloch–Torrey equation are also used to investigate diffusion in the same geometric models and compare their results with theoretical predictions from analytical theory and experimental data.

The accuracy of the relationships between ADC and structural dimensions for typical diffusion gradient timing parameters and gradient strengths used in ^{3}He lung MR is also assessed in this work. Particular attention is paid to the case where strong diffusion gradients are applied, resulting in non-Gaussian diffusion behaviour (i.e. the localized diffusion regime), which has generally been overlooked in the ^{3}He lung MR literature. Finally, the implications of the experimental results obtained here for in vivo lung morphometry using ^{3}He MR are discussed.

2. Background theory

In this section the basic theory of MR diffusion is briefly presented to aid the understanding of this paper. More detailed accounts of this theory can be found elsewhere (e.g. [13,14] and references within). The theoretical basis and corresponding equations of the cylinder model are introduced later.

2.1. Diffusion regimes

The behaviour of the MR signal in PGSE diffusion experiments is determined by the geometry and size of the compartment in which diffusion occurs and the timing parameters and strength of the diffusion sensitization gradients. The relationship between these is best explained in terms of three length scales [13,15]: l_S, l_D and l_G. The structural length l_S is the characteristic size of the confining structure ($l_S = R$ for a cylinder). The one-dimensional diffusion length ($l_D = \sqrt{2D_0\Delta}$, where D_0 is the free diffusion coefficient) is the average distance travelled by one particle (helium atom) within the diffusion time Δ. The gradient dephasing length l_G is the average length that a spin must diffuse within a field gradient G in order to dephase by 2π radians with respect to a stationary spin and is given by:

$$l_G = (D_0/\gamma G)^{1/3} \quad (1)$$

where γ is the gyromagnetic ratio.

Fig. 1 shows a schematic diagram of the three asymptotic diffusion regimes and their dependence on the relative sizes of the three characteristic length scales. In the free diffusion ($l_D << l_S, l_G$) and restricted diffusion ($l_S << l_D, l_G$) regimes, the phase distribution is approximately Gaussian and the transverse magnetization within the confining structure is nearly uniform. The diffusion signal decay is then monoexponential and described as:

$$S(b) = S_0 \exp[-b\ \mathrm{ADC}] \quad (2)$$

where b is the diffusion weighting, which depends on the diffusion gradient intensity and timing parameters. In the free diffusion regime, the ADC is constant and equal to D_0. In the restricted diffusion regime, the ADC depends on the geometry and dimensions of the confining structure and the diffusion time Δ, but is independent of the gradient amplitude. Analytical expressions relating ADC and l_S in this regime have been obtained for simple geometries (e.g. parallel plates, cylinder, sphere) using the Gaussian phase approximation (for an excellent review see [13]).

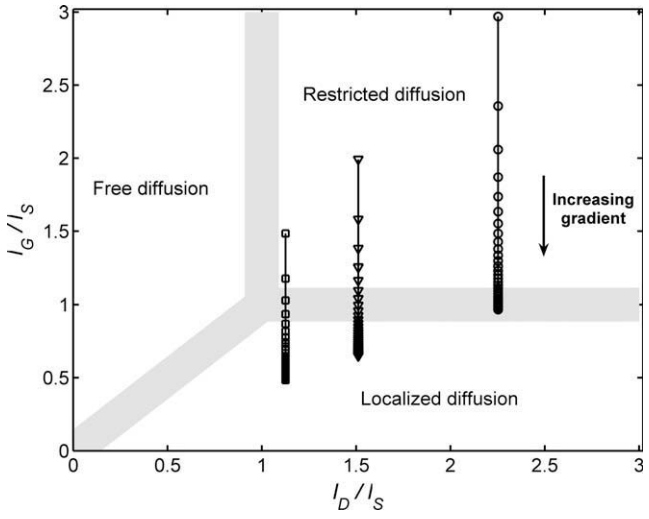

Fig. 1. Schematic diagram of the three diffusion regimes; the approximate boundaries between the regimes (i.e. intermediate regimes) are shown approximately as shaded areas. The trajectories shown correspond to three diffusion acquisitions (presented in Section 4.2) for 0.5 (circles), 0.76 (triangles) and 1 mm (squares) diameter tubes (G = 1–30 mT/m, Δ = 1.8 ms, D_0 = 0.92 cm^2/s).

The localization regime [15] corresponds to the case where l_G is the shortest length scale ($l_G << l_S,\ l_D$). In this regime, the phase distribution strongly deviates from a Gaussian distribution, the transverse magnetization is non-uniform and the observed signal originates mostly from regions within a distance l_G from restricting boundaries perpendicular to the applied diffusion gradient (edge enhancement effect [25,26]).

2.2. Anisotropic diffusion

Anisotropic structures, where diffusion is restricted in a different manner in different directions are frequently found in nature. Callaghan et al. [16] studied diffusion in samples that can be approximated by many randomly oriented cylinders such as long polymer chains and endosperm tissue of wheat grains. Assuming Gaussian phase distribution, the signal obtained from a single cylinder, whose axis forms an angle ϕ with the direction of the diffusion sensitizing gradient, follows a monoexponential decay with ADC as given by [16]:

$$\mathrm{ADC}\ (\phi) = D_L\ \cos^2\ \phi + D_T\ \sin^2\ \phi \tag{3}$$

where D_L and D_T are the longitudinal and transverse ADC's measured with the gradients oriented parallel and perpendicular to the cylinder axis, respectively.

The signal attenuation resulting from a large number of isotropically oriented non-connected cylinders can then be obtained by integration with uniform weighting over all solid angles [16]:

$$\frac{S(b)}{S_0} = \frac{\int_0^{\pi} \exp\left[-b(D_L\ \cos^2\ \phi + D_T\ \sin^2\ \phi)\ \sin\ \phi\right] \mathrm{d}\phi}{\int_0^{\pi} \sin\ \phi\ \mathrm{d}\phi} \tag{4}$$

2.3. Cylinder model

The approach of Callaghan (previous section) was adopted by Yablonskiy et al. [7] to model the diffusion of ^{3}He in lung acinar airways. The model assumes that for short term diffusion (i.e. diffusion time less than ~5 ms) the effects of branching nodes and alveolar sac endings can be neglected and thus alveolar ducts can be considered as long non-connected cylinders of random orientation.

The behaviour of the ^{3}He MR diffusion signal (originating from an imaging voxel containing many isotropically oriented cylinders) was obtained from the integration of Eq. (4), which results in:

$$S(b) = S_0 \exp(-b\bar{D})\left(\frac{\pi}{4bD_{AN}}\right)^{1/2} \exp\left(\frac{bD_{AN}}{3}\right)\ \Phi\left[(bD_{AN})^{1/2}\right] \tag{5}$$

where $\Phi(x)$ is the error function, and D_{AN} and $\bar{D}$ were defined as:

$$D_{AN} = D_L - D_T \tag{6}$$

$$\bar{D} = \frac{D_L}{3} + \frac{2D_T}{3} \tag{7}$$

Eq. (5) suggests that the non-monoexponential signal decay, observed in ^{3}He lung MR diffusion experiments, results from superposition of the monoexponential signals originating from Gaussian diffusion in each of the individual airways. It is important to highlight that the reliance of Eqs. (3) and (5) on the assumption of Gaussian diffusion [16], and the limitations that this assumption imposes on the validity of this model have not been acknowledged in the published papers related to the cylinder model.

MR diffusion data from in vivo lung experiments was then fit to Eq. (5) to obtain D_L and D_T. The cylinder radius R was then estimated from D_T using the following relation [7]:

$$D_T = \frac{4R^4}{D_0\Delta^2\ w(\tau/\Delta)} \sum_j \frac{\beta_{1j}^{-4}}{\beta_{1j}^2 - 1}\ Q(\beta_{1j}^2\ D_0\Delta R^{-2},\ \tau/\Delta) \tag{8}$$

where β_{1j} is the jth (nonzero) root of the equation $J_1'(x) = 0$ (J_1 is the first order Bessel function) and the functions w and Q are defined in [7] and depend on the timing parameters (Δ and τ) of the diffusion sensitization gradients (see Fig. 2). Since within an imaging voxel there are alveolar ducts of different radii covered by an alveolar sleeve, R is interpreted as an effective duct radius. For negligible ramp time τ, Eq. (8) reduces to the well known expressions for the ADC in cylindrical geometry [13,27] obtained in the context of diffusion in porous media. Note that Eq. (8) also assumes Gaussian phase distribution and suggests that the ADC depends on the cylinder radius and the timing parameters of the diffusion gradient but not on the gradient strength.

2.4. Updated cylinder model

The cylinder model was later updated [18] in an attempt to account for non-Gaussian effects. The new model incorporates a more complex geometry that includes alveoli and uses Monte Carlo simulations to obtain relationships between the geometric properties of the model and the diffusivities D_L and D_T which depend on the b-value.

For a smooth tube (i.e. $r = R$ in the equations from [18]), $D_L = D_0$, and D_T is given by:

$$D_T = D_{T0} + b\beta_T\ D_{T0}^2 \tag{9a}$$

where D_{T0} and β_T are given by:

$$D_{T0} = 0.44\ D_0\ K^{[0.1K^{-3/2}]} \tag{9b}$$

$$\beta_T = 0.09\ K^{[1-K^{0.7}]} \tag{9c}$$

and $K = R/(\sqrt{2}l_D)$.

Note that the updated model only introduced a linear correction for the b-value dependence (Eq. (9a)) of the relationships between diffusivities for single airways with gradients directed parallel or perpendicular to the airway axis. These relationships (e.g. Eqs. (9) for a smooth cylinder) are then used in the new model together with Eq. (5) to fit the diffusion data and obtain estimates of D_{T0} and β_T from which airway dimensions can be calculated. Since the updated model still relies on Eq. (5) which was obtained under the assumption of Gaussian phase approximation, the validity of the model is still limited by the validity of this assumption.

The updated model does not account for any angular dependence of the apparent diffusivities and orientation-dependent non-Gaussian diffusion effects, since it still uses Eq. (3) to describe

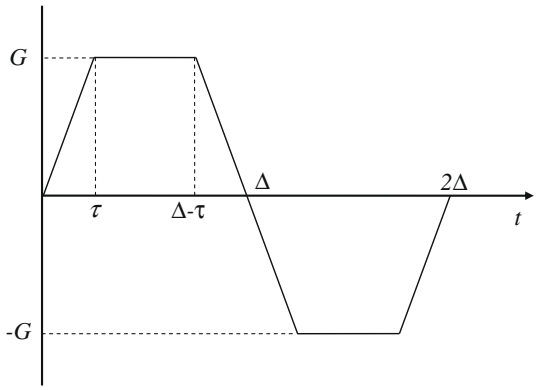

Fig. 2. Diagram of the waveform of the diffusion sensitization gradient used in this work (τ = 0.5 ms, Δ = 1.8 ms). The b-value corresponding to this gradient waveform is given by: $b = (\gamma G)^2\ [2/3\ \Delta^3 + \tau\ (\Delta^2 + 1/6\ \Delta\tau - 8/15\ \tau^2)]$.

the angular dependence of the ADC. There is a fundamental contradiction within this model when non-Gaussian effects are partially taken into account in the relationship between the diffusivities and airway dimensions with gradients directed parallel or perpendicular to the cylinder axis, while the angular dependence of the ADC of a single airway is described with an expression which is only valid for Gaussian diffusion.

Also note that although Eq. (9a) introduces a linear dependence of D_T on the b-value, D_T does not depend separately on the gradient strength G, and diffusion time, Δ. Different combinations of G and Δ, which produce the same b-value, could result in diffusion experiments occurring in different diffusion regimes, with different signal behaviours. It has been shown that timing and gradient strength both affect the ADC but in different ways [11]. Furthermore, Eq. (9a) is only valid for $R < 0.5$ mm; for larger R, the linear approximation is not valid and terms proportional to b^2 or higher are needed [18].

This work concentrates on testing the fundamental physical basis of the cylinder models (i.e. original and updated cylinder model) since a more complete analysis should test other important assumptions (e.g. geometry, boundary conditions) whose limits of validity have not yet been experimentally investigated in appropriate physical models. This investigation will be the subject of future work.

3. Methods

To investigate the limits of validity of the physical basis of the cylinder model and the accuracy of cylinder radius estimates (i.e. Eqs. (2), (3), (5), (8), and (9)), a number of experiments and computer simulations in well defined geometries were performed. In the next section these experiments and computer simulations are described along with the MR hardware and phantoms used.

3.1. MR hardware and pulse sequence

All experiments were performed on a 3T Philips Intera whole body system, using a custom-built transmit-receive birdcage coil (15 cm diameter), tuned to the ^{3}He resonance frequency (97 MHz) and operated in linear mode with a custom-built T/R switch.

Global ADC data were obtained by FID acquisition following bipolar diffusion gradients with a modified 2D spoiled gradient-echo sequence (readout and phase encode gradients turned off). The diffusion gradient timing parameters (Fig. 2) were the same as those used in [7], with 0.5 ms ramp time, 1.8 ms pulse duration (i.e. plateau time: 0.8 mm) and no delay between pulses.

The gradient strength G was varied in 60 equal steps from -30 to 30 mT/m. This way diffusion data for each b-value was obtained twice with reversed polarity gradients (i.e. one acquisition with first gradient lobe negative and second positive and another acquisition with first lobe positive and the second negative). This double acquisition scheme permits the assessment of potential errors in the applied gradients. These could result for example from a background B_0 gradient or a DC off-set in the pulsed gradients. It also allows verification of the accuracy of the flip angle calibration, since each pair of acquisitions with same gradient strength is separated by a different known number of RF pulses, and assessment of any effect from decreasing SNR due to RF depletion. Care was taken to completely depolarize any ^{3}He gas remaining in the phantom tubes between experiments (through repeated RF pulse irradiation).

3.2. Phantoms and hyperpolarized gas

The phantoms (Fig. 3a and b) were built from Ethyl Vinyl Acetate tubing with inner diameters 0.5, 0.76 and 1 mm (tolerance ± 0.005 mm) available from Harvard Apparatus (Kent, UK). The first phantom (“*phantom A*”, Fig. 3a) consisted of three bundles (one of each tube diameter) of straight parallel tubes (16 cm long). The second phantom (“*phantom B*”) consists of 100 turns of tubing of each diameter wound on the surface of a cylinder of diameter 6 cm (Fig. 3b). Hyperpolarized ^{3}He can be delivered to tubes of different diameter independently by means of plastic syringes (after evacuation of air) via Luer–Lock connections. The syringes where detached from the phantoms just before starting the acquisition to allow for pressure equalization to normal atmospheric pressure (room temperature ~19°).

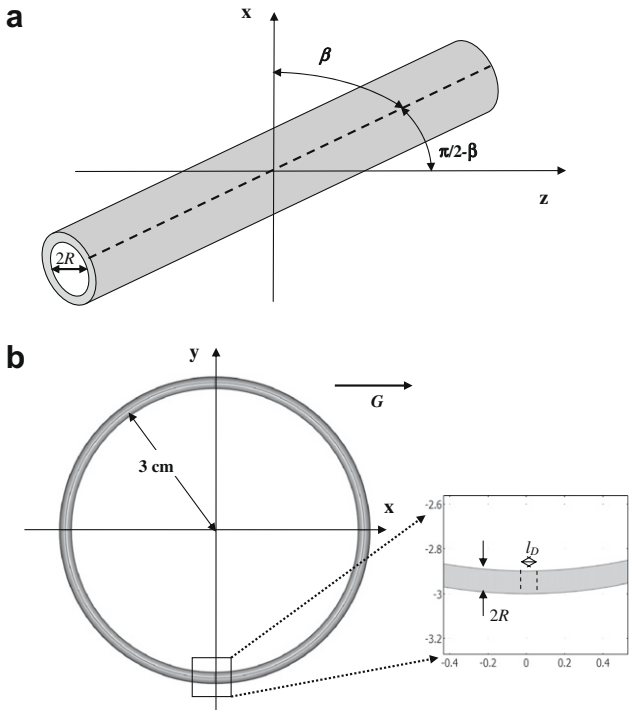

Fig. 3. Diagrams of the phantoms A and B used in this work. Here a single tube is shown for clarity, the actual phantoms consisted of several parallel tubes (a), or circular turns (b). The inset in (b) shows that the curvature of the tubes in phantom B is negligible over the diffusion lengths present in this work (axis in cm).

^{3}He with a polarization of ~25% was obtained using a Helispin Rubidium Spin-Exchange polarizer (GE Healthcare, USA) and mixed with N_2 in different gas mixtures. The ^{3}He concentration in those gas mixtures were within the range (~20–100%) typically used in lung MR experiments.

The free diffusion coefficients D_0 of these gas mixtures were determined from diffusion MR experiments (as described in Section 3.2) in a 60 ml syringe. The diameter of the syringe (3 cm) is much larger than the largest diffusion length expected in the experiments ($l_D \approx 0.8$ mm). D_0 of the gas mixture in the syringe was measured before each experiment where a new batch of gas was used, to account for any errors in the preparation of the mixture. All the b-values in each experiment were obtained with a single filling of gas.

3.3. Experiments with phantom A (validation of Eqs. (2), (3), (8) and (9))

Phantom A was positioned inside the magnet with the tube axis parallel to the horizontal (x–z) plane and forming an angle β with the x-axis (see diagram of Fig. 3a). The phantom could be accurately geometrically aligned aided by the MR system alignment lasers and a surface bubble spirit level attached to the phantom. The

slice thickness (3–5 cm) was selected to avoid excitation of the ends of the phantom (i.e. where the tubes are curved), while keeping the volume of gas diffusing in and out of the slice edges negligible with respect to the volume of the bulk of the excited spins.

In the first experiment, diffusion acquisitions were performed (as described in Section 3.1) for each tube diameter and $\beta = 0°$ (i.e. gradient in x direction and tubes parallel to z-axis). Diffusion data from each acquisition was fitted to a monoexponential to obtain a single ADC value. Since for $\beta = 0°$ the ADC = D_T, as such R was estimated from the ADC using Eq. (8). This experiment tests the assumption that the signal decay from a diffusion experiment with the gradient perpendicular to the axis of a single cylinder is monoexponential (i.e. follows Eq. (2)) and its ADC is accurately defined by Eq. (8). Experimental results were also compared to the model of Eqs. (9)

To test the validity of Eq. (3), different angles β (see diagram of Fig. 3a) were used. Two sets of diffusion acquisitions were then performed for each angle with the diffusion sensitizing gradient oriented along the x- and z-axes, respectively. This way, two ADC values (D_x = ADC (β) and D_z = ADC ($\pi/2 - \beta$), respectively) could be obtained for each angle β. From Eq. (3), the following relation can be obtained for this scenario:

$$D_z + D_x = D_L + D_T$$

and since for a long cylinder $D_L = D_0$, D_T can be obtained as:

$$D_T = D_z + D_x - D_0 \tag{10}$$

This result indicates that if Eq. (3) is valid, D_T can be then estimated (using Eq. (10)) from two acquisitions with orthogonal gradients and this estimate should be independent of the angle β and the gradient strength.

3.4. Experiments with phantom B (validation of Eq. (5))

To test the validity of Eq. (5), diffusion signals were acquired from phantom B with the diffusion sensitization gradient perpendicular to the axis of phantom B (i.e. parallel to the plane of the circular turns, Fig. 3b). Due to the large diameter of the turns in phantom B compared to the tube diameters (see inset in Fig. 3b), the curvature of the tubes over a length equal to the diffusion length ($l_S < 1$ mm) can be neglected and a full loop can be considered equivalent to a collection of elemental long cylinders uniformly distributed with orientations in all possible (2D) angular directions.

Following the approach of Callaghan et al. [16], an analytical expression for the diffusion signal originating from this geometric phantom can be written as [11]:

$$\frac{S(b)}{S_0} = \frac{\int_0^{\pi} \exp\left[-b(D_L \cos^2\phi + D_T \sin^2\phi)\right] d\phi}{\int_0^{\pi} d\phi} \tag{11}$$

This expression is now integrated (See Appendix) to obtain:

$$\frac{S(b)}{S_0} = \exp(-b\bar{D}_{2D})\, I_0\left(\frac{bD_{AN}}{2}\right) \tag{12}$$

where $I_0(x)$ is the zeroth order modified Bessel function of the first kind, D_{AN} is given by Eq. (6) and $\bar{D}_{2D}$ is defined as:

$$\bar{D}_{2D} \equiv \frac{D_T}{2} + \frac{D_L}{2} \tag{13}$$

Since $I_0(0) = 1$ for $D_{AN} = 0$, the signal decay in Eq. (12) becomes monoexponential. For $D_{AN} > 0$, $I_0(x)$ is an exponentially increasing function and the signal decay is increasingly slowed down (with increasing b-value) and deviates further from the monoexponential.

Eq. (12) is the equivalent of Eq. (5) in two dimensions and will be used to fit the diffusion data obtained from the experiments with phantom B to obtain estimates of D_T and D_L. To test the ability of the cylinder model to estimate the airway dimensions from the MR diffusion signal, R can then be calculated from D_T using Eqs. (8) and (9) and compared to the known nominal radius of the tubes.

3.5. Computer simulations

Computer simulations were performed by numerically solving the Bloch–Torrey equations [19,28] using a finite element method for computer models of phantoms A and B and the diffusion sensitizing gradient waveform of Fig. 2. Boundary conditions assumed impenetrable walls (zero flow through the walls) on all surfaces [28].

The geometric models were created using Comsol Multiphysics (COMSOL AB, Stockholm, Sweden) and then exported to Matlab (MathWorks, Natick, MA), where the solutions for the transverse magnetization dephasing for each b-value and tube diameter were calculated. From the obtained transverse magnetization distribution, the ADC could be estimated after integration over the tube volume.

To avoid effects from the finite length of the cylinder when simulating experiments with the straight tubes, only a 1 mm long section at the centre of the cylinder was used in the integration for signal calculation and estimation of the ADC. Between 60 and 100 b-values were used in the simulations for each tube diameter. The longest time taken for the simulations of a single tube diameter was approximately 20 min on a modern laptop PC (Intel Core2 processor at 2.0 GHz, 2 Gb RAM).

The results of the simulations were compared to the theoretical predictions of the cylinder model and the experimental results. They were also used to provide further physical insight into the microscopic distribution of the transverse magnetization inside the tubes (which is beyond the resolution limits of MRI experiments).

4. Results and discussion

4.1. Estimation of D_0

Fig. 4a and b show the measured diffusion signal decay and the estimated ADC as functions of the b-value for ^{3}He gas (gas mixture: 100% ^{3}He) diffusing in a 60 ml syringe (i.e. 3 cm diameter cylinder). Fig. 4a shows a deviation of the signal decay from the straight line (log-scale plot) corresponding to the monoexponential behaviour expected in free diffusion. It can be observed in Fig. 4b that the ADC only remains approximately constant (as expected for free diffusion) for b-values below $\sim$2 s/cm^2 ($G < 15$ mT/m) and then starts to decrease.

To avoid the effects of non-monoexponential behaviour of the signal for large gradients, D_0 was estimated from the first part of the signal decay curve ($b < 2$ s/m^2) within the limits of free diffusion for the syringe (Fig. 4a). The estimated D_0 values ranged between 0.87 (for 20% ^{3}He) and 1.86 cm^2/s (for 100% ^{3}He). The corresponding diffusion lengths l_D range between 0.58 and 0.82 mm. The D_0 estimate for 100% helium is in good agreement with the previously reported [13] experimental value of 1.84(8) cm^2/s (after correction for pressure difference). The D_0 estimate for 20% helium also agrees with the theoretically calculated binary diffusion coefficient [29] of 0.90 cm^2/s.

The behaviour of the signal decay and the ADC observed in Fig. 4 indicates the on-set of the localization regime as the gradient strength increases. As the diffusion goes from the free to localized regime most of the observed signal originates from regions near the boundaries. These results (which are similar to those reported in [15] for water diffusion between parallel plates) are significant because they represent a deviation from monoexponential behaviour for diffusion in a relatively large confining space ($l_S \approx 15$ mm,

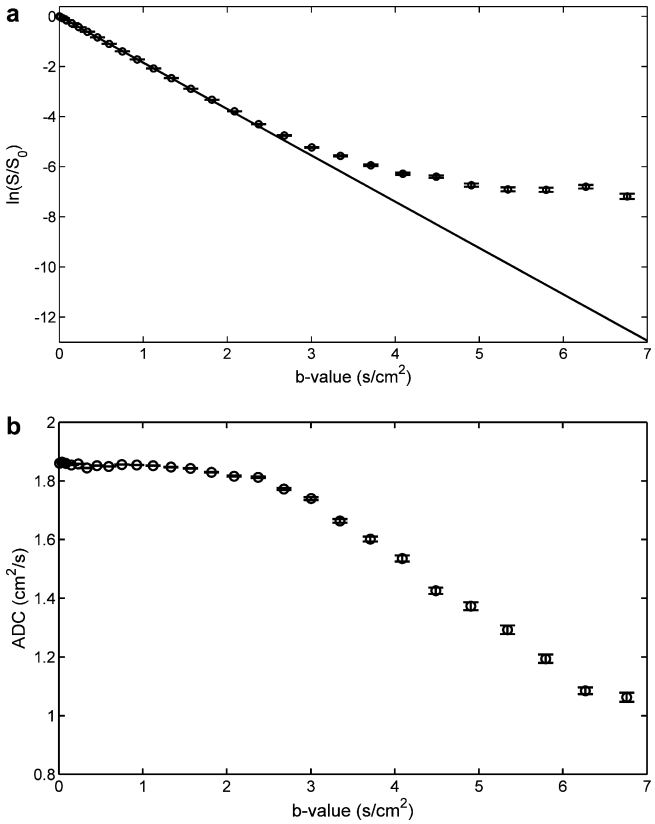

Fig. 4. Results of diffusion experiments for D_0 estimation. Dependence of the (a) diffusion signal decay and (b) the estimated ADC (ADC $(b) = -1/b \ln(S(b)/S_0)$ on the b-value for the gas mixture B (100% ^{3}He) in the 60 ml syringe. The solid line in (a) is the fit to a monoexponential function of the data for $b < 2$ s/cm^2.

$l_D \approx 0.8$ mm), for gradient intensities commonly used in lung ADC experiments [7,9,30]. As a consequence, for such gradient intensities, the effect of boundaries, albeit separated by a distance larger than the diffusion length, cannot be neglected in the treatment of the signal behaviour. This is indeed the case for acinar airway branching nodes and alveolar sac endings whose effects are assumed to be negligible in the cylinder model, but may significantly contribute to the non-monoexponential behaviour of the signal. Experimental and theoretical investigation of the limits of validity of this assumption is needed and will be the subject of future work.

4.2. Experiments with phantom A (validation of Eqs. (2), (8) and (9))

In Fig. 5, the signal decay from experiments with phantom A are presented as a function of the b-value and compared with the estimates from theory (Eqs. (8) and (9)) and from our computer simulations. For the narrowest tubes (0.5 mm diameter), the signal decay is nearly monoexponential for all b-values, consistent with the restricted diffusion regime (see trajectory in diagram of Fig. 1), since l_S is smaller than (or nearly equal to) the minimum dephasing length corresponding to the maximum gradient strength: $l_G \approx 0.25$ mm for $G = 30$ mT/m ($\sim$8 s/cm^2).

For the larger diameter tubes, the signal decay (Fig. 5) significantly deviates from monoexponential behaviour (i.e. ADC increases) with increasing b-values. Diffusion in the 0.76 mm diameter ($l_S = 0.38$ mm) tubes, for b-values above $\sim$1 s/cm^2, occurs in the intermediate regime between restricted diffusion and localized diffusion (Fig. 1). For the 1 mm diameter ($l_S = 0.5$ mm) tubes diffusion across almost the whole b-value range occurs in the localization regime (Fig. 1), and for the highest b-values $l_G \approx 0.5\ l_S$.

The results of the computer simulations are in relatively good agreement with the experimental results demonstrating the deviation from Gaussian diffusion. The observed difference between experiment and simulation results could be attributed to small misalignments of the tubes due to construction errors. Susceptibility-induced background gradients, which are known to affect the ADC measurements [31] could also have contributed. Investigation of the effects of these susceptibility-induced gradients in ADC experiments is important and will be the subject of future work with numerical simulations in these well defined geometrical phantoms.

The theoretical signal behaviour predicted by Eqs. (9) are in good agreement with the experimental data and the signal behaviour obtained from our simulations. These results suggest that the new model of Eqs. (9) correctly describes non-Gaussian diffusion effects in smooth tubes in experiments with gradients perpendicular to the tube axis, for the tube radii, gradient strengths and timing

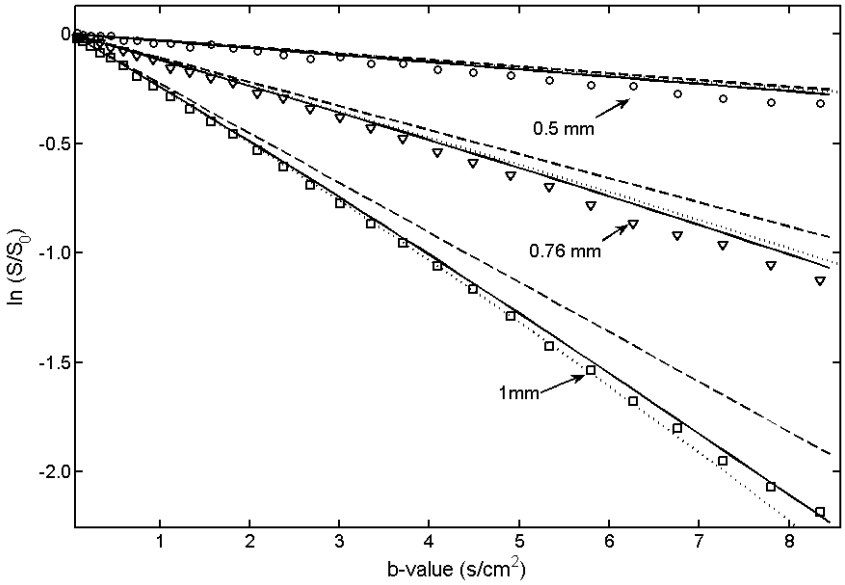

Fig. 5. Comparison of signal decays obtained from experiments with phantom A (for the 0.5, 0.76 and 1 mm diameter tubes) to the theoretically predicted behaviour (Eq. (8), dashed line; Eqs. (9), dotted lines) and numerical simulations (solid lines). Error bars have been omitted for clarity (see Fig. 4 for typical errors).

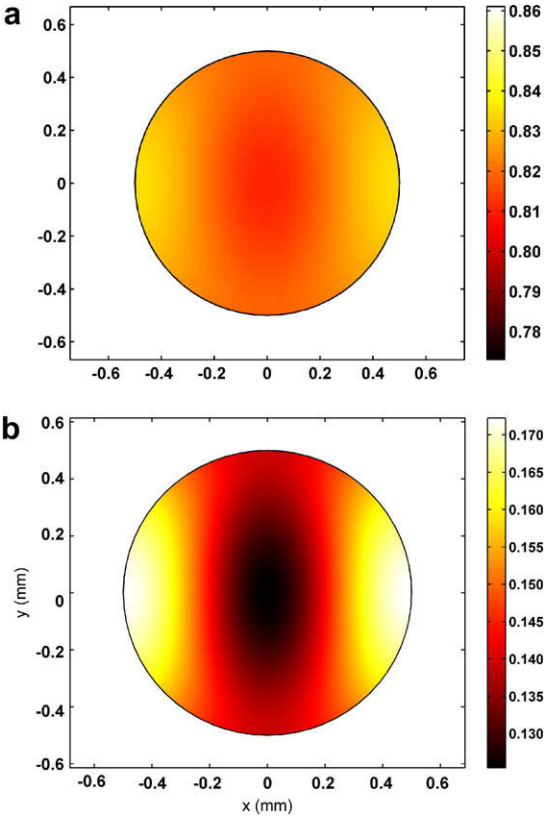

Fig. 6. Computer simulation of experiments with phantom A ($R = 0.5$ mm, gradient in x direction). The transverse magnetization (M_{xy}) distributions after 10 mT/m (a) and 30 mT/m (b) diffusion sensitization gradients are shown (initial condition, M_{xy} ($t = 0$) = 1). Strong edge effects (localized diffusion) are visible in (b) while magnetization distribution is nearly uniform in (a). Note the difference in the scales (in relative values) chosen to highlight the slight signal variation in (a), otherwise invisible.

parameters used in this work. Validation of this model over a larger range of gradient parameters (i.e. strength and timing parameters) and airway sizes and for more complex structures is still necessary.

In Fig. 6, the simulated spatial distribution of the transverse magnetization in the plane of the tube cross-section is shown for small and large diffusion gradient strengths whose direction is oriented left to right. The edge enhancement effect is more evident for tubes of larger diameter for the largest gradient strength, a trend confirmed by the observation of the largest deviation from mono-exponential signal decay for the largest diameter tubes in Fig. 5.

Table 1 shows the tube diameters calculated (using Eq. (8)) from the fit of the experimental diffusion data using the original and updated cylinder models. The diameters calculated using Eq. (8) are consistently larger than the known nominal diameters of the tubes. The discrepancies are larger for larger b-values (i.e. larger gradient strengths) and larger tube diameters. These results agree with our previously published predictions from simulations [19], that the original cylinder model systematically over-estimates the airway diameter and also identify the breakdown of the Gaussian approximation (in the on-set of localized diffusion) as a likely source of this over-estimation. The diameters estimated using the updated cylinder model (Eqs. (9)) are in better agreement with the nominal diameters; the remaining discrepancies do not change with gradient strength and are likely due to the experimental uncertainties described above.

Table 1
Comparison of tube diameters estimated from experiments with phantom A (using Eqs. (8) and (9)) with the known nominal diameters at three different b-values ($D_0 = 0.92 \pm 0.03$ cm^2/s). The relative error for the experimental diameter estimates was always less than 5%.

Nominal tube diameter (±0.005 mm)	Estimated tube diameter (original/updated model, in mm)		
	$b = 1$ s/cm^2	$b = 3$ s/cm^2	$b = 8.3$ s/cm^2
0.510	0.532/0.536	0.548/0.540	0.544/0.538
0.760	0.788/0.779	0.792/0.781	0.810/0.782
1.020	1.058/1.041	1.063/1.030	1.080/0.996

Table 2
Results of the experiments with phantom A ($D_0 = 0.88 \pm 0.02$ cm^2/s) for two different angles β and a $G = 25$ mT/m. The transverse diffusivity D_T estimated from the experiments using Eq. (10) is compared to the theoretical values (independent of β) calculated with Eq. (8). The relative error for the experimental D_T estimates was always less than 9%.

Nominal tube diameter (mm) (±0.005 mm)	D_T (cm^2/s)			
	$\beta = 58°$	$\beta = 78°$	$\beta = 90°$	Theory
0.510	−0.151	0.042	0.039	0.029
0.760	−0.108	0.136	0.133	0.113
1.020	0.026	0.282	0.262	0.218

The results presented here demonstrate the non-Gaussian nature of diffusion in a single cylinder for gradient strengths typically found in lung ADC experiments, for which the Gaussian approximation is not valid. This means that for such gradients the concept of an ADC, and hence Eqs. (2) and (3) have no meaning even for a single airway.

4.3. Experiments with phantom A (validation of Eq. (3))

Table 2 shows the results of the estimation of D_T using Eq. (10) for two angles ($\beta \approx 58°$ and 78°). These results show that the estimated D_T values are not independent of β as predicted by Eq. (10) and in some cases even become negative (see Fig. 7), which is physically impossible. This occurs at lower b-values for the tubes of smaller diameters (Fig. 7), since the actual values of D_T are small and small deviations in the diffusion behaviour (i.e. non-Gaussian effects) would make the estimated D_T negative. In Fig. 7, the predicted behaviour of D_T as a function of b-value from Eqs. (8) and (9) have been plotted for comparison. Neither the original nor

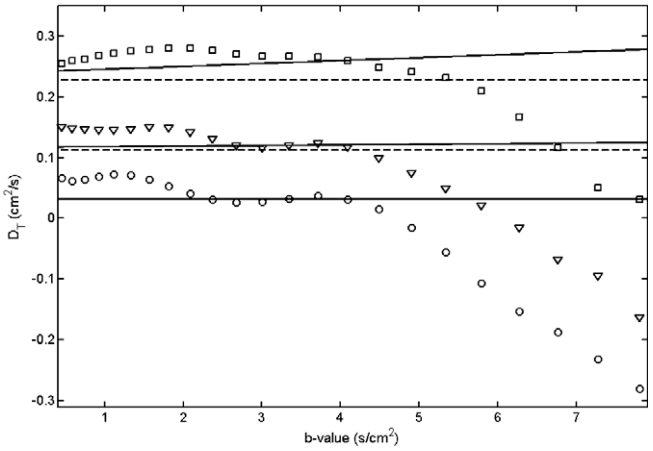

Fig. 7. D_T values (estimated using Eq. (10)) as a function of the b-value for different tube diameters (squares: 1 mm, triangles: 0.76 mm and circles: 0.5 mm) and $\beta = 58°$. The dashed lines and solid lines show the theoretical D_T values calculated using the original cylinder model, Eq. (8), and the updated cylinder model, Eqs. (9), respectively. D_T becomes negative for high b-values (i.e. large gradient strength).

the updated model include any angular dependence of the non-Gaussian effects and hence cannot describe the experimental data obtained here. The linear b-value dependence of D_T introduced in the updated cylinder model from Monte Carlo simulations (with a single gradient orientation) cannot account for the angular dependent effects shown in Fig. 7.

Fig. 8 shows the signal distribution in cross-sections of the tubes, perpendicular to the x–z plane and parallel to the gradient direction, that results from simulations of ^{3}He diffusion in a computer model of phantom A ($R = 0.25$ mm, $G = 30$ mT/m). These cross-sections are ellipses whose major axis L is parallel to the gradient direction and increases ($L \propto R/\sin\delta$) as δ (angle between the gradient direction and the cylinder axis) decreases from 90° to 0°

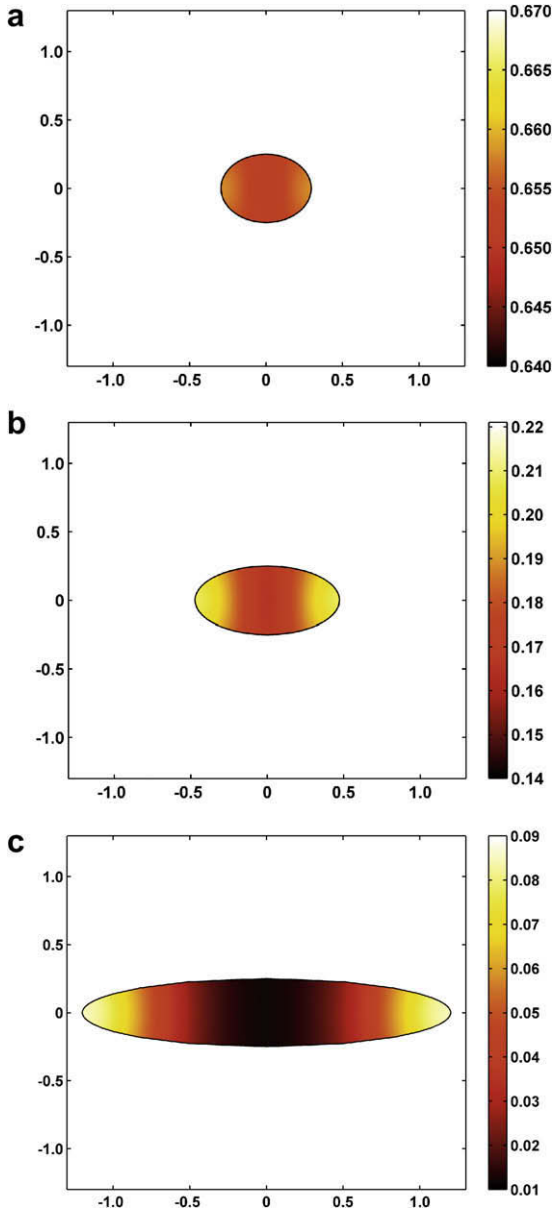

Fig. 8. Results of simulations of diffusion experiments with a computer model of phantom A (tube diameter 0.5 mm) and a gradient ($G = 30$ mT/m) forming an angle δ of (a) 58°, (b) 32° and (c) 12° with the cylinder axis (parallel to z-axis). The transverse magnetization (M_{xy}) distribution is shown in 2D cross-sections (dimensions in mm) parallel to the gradient direction (initial condition, $M_{xy}(t = 0) = 1$). The cross-sections are ellipses whose major semi-axis L increases with increasing δ ($L \propto R/\sin\delta$). Note the difference in the scales (in relative values) chosen to highlight the slight signal variations in (a) and (b), otherwise invisible.

(due to symmetry the angular behaviour in other quadrants is the same). It can be seen that in Fig. 8a the edge effects are almost invisible and nearly uniform signal originates from most of the cylinder volume (i.e. cross-section area). As the angle decreases (Fig. 8b and c), the fraction of the cylinder volume that contributes negligible signal increases. The diffusion signal in these cases becomes less sensitive to the volume, being strongly dependent on edge effects and thus more influenced by the surface area perpendicular to the gradient.

As the gradient strength increases in these experiments, the relationship between the three length scales changes and diffusion may occur in the localization regime or one of the intermediate regimes, depending on the diffusion time, tube radius and angle (see trajectories in Fig. 9a). This is clearly demonstrated in Fig. 10, where differences in signal behaviour for gradients in the x and z directions can be observed. These deviations from monoexponential decay are the result of the transition between different diffusion regimes (Fig. 9a). For a gradient in the x direction (Fig. 10a), diffusion goes from the restricted to the localized regime and the signal starts to decay faster than a monoexponential, leading to an ADC value larger than expected from theory (similar to the behaviour shown in Section 4.2). For a gradient in the z direction (Fig. 10b), diffusion goes from the free to the localized regime and hence the signal decay slows down and the apparent D_L be-

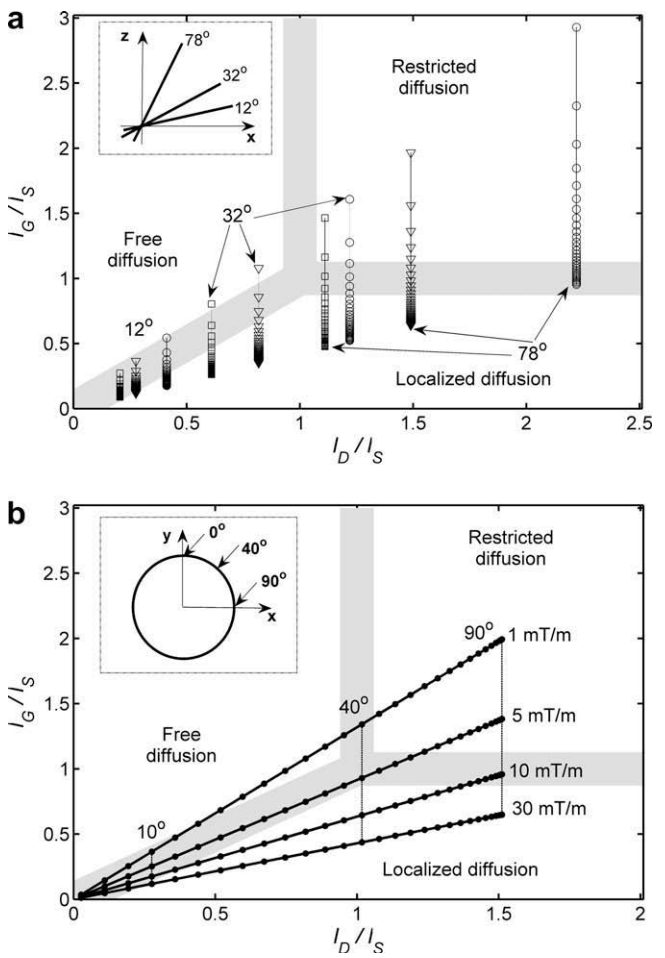

Fig. 9. Diagram of diffusion regimes of the different diffusion weighted experiments performed showing the trajectories corresponding to experiments with (a) phantom A for the 0.5 (circles), 0.76 (triangles) and 1 mm (squares) diameter tubes, with diffusion gradient along x direction, and (b) phantom B for the 0.76 mm tube only, with gradient along y direction. Note that $l_S = R/\sin\beta$. The dots in the trajectory lines in (b) represent angular positions (with constant 3° spacing) in the phantom.

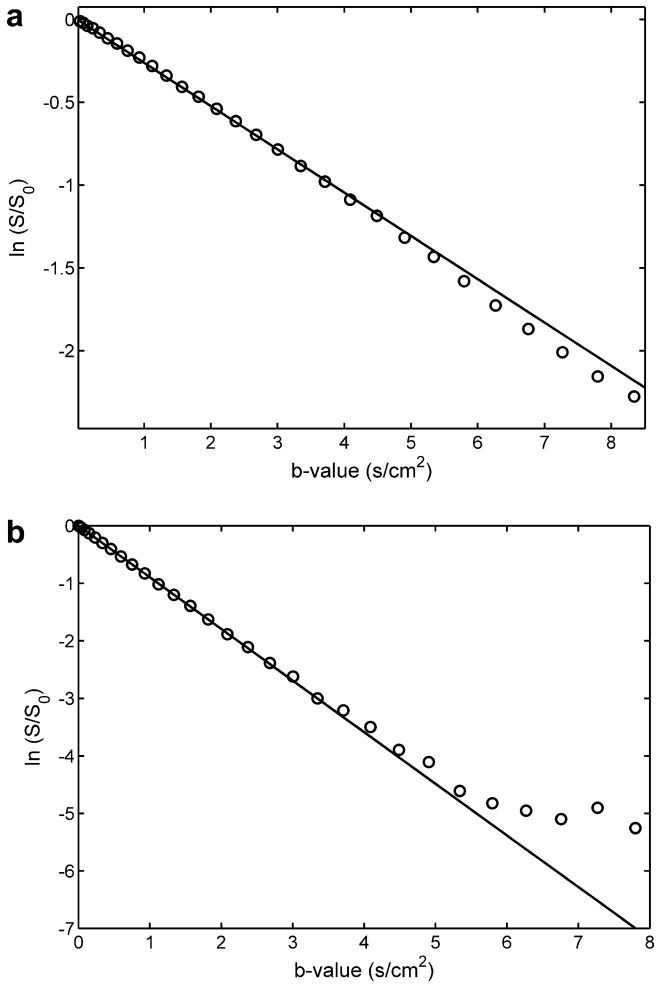

Fig. 10. Diffusion signal behaviour from experiments with phantom A ($\beta = 78°$) and diffusion sensitization gradients in (a) x and (b) z directions (tube diameter 1 mm). Monoexponential fits (to data in range $b < 2$ s/cm^2) are shown as solid lines. Error bars not shown as they were smaller than the symbols.

comes smaller than D_0 (similar to behaviour observed in Section 4.1). Note that the signal behaviour of Fig. 10b, cannot be explained using the updated cylinder model (Eqs. (3) and (9)), since $\beta_T > 0$ and $\beta_L = 0$ for a smooth cylinder.

These results indicate that Eq. (3) breaks down when $l_G \leqslant l_D$ (i.e. in the localized regime and its neighbouring intermediate regimes). In the intermediate regime between free and restricted diffusion, it has been shown [13] that the signal behaviour can still be described by a monoexponential decay with the ADC predicted from the Gaussian approximation. Hence in this intermediate regime Eq. (3) is expected to hold.

When Eq. (3) is not valid, then Eq. (4) can not be used to calculate the bulk signal, since the signal coming from an individual cylinder deviates from Gaussian behaviour and hence can no longer be characterized with a single D_T value for all angular orientations. Even when diffusion is exponential with the gradient perpendicular to the tube axis, for other angles the structural length l_S (for the elliptical cross-section) could become comparable or larger than l_G (depending on the gradient strength), resulting in non-exponential signal behaviour. This implies that the uniform weighting for all angular directions (Eq. (4)), implicit in the cylinder model, would also no longer be valid for all gradient strengths.

These results demonstrate that the changes introduced to the cylinder model by Sukstanskii et al. in [18] are not able to account for the non-Gaussian effects described in this section. The new expressions for the diffusivities D_T and D_L were obtained with gradients perpendicular and parallel to the axis of their airway model, respectively, and therefore did not account for any angular dependence. The angular dependence of the non-Gaussian diffusion effects may be incorporated into an improved version of the cylinder model using computer simulations as we previously showed in [11,19]. The signals obtained from simulations with a number of gradient angular orientations uniformly distributed are added to obtain the bulk voxel signal, from which relationships between diffusivities and airway may be extracted. This would account for orientation-dependent non-Gaussian effects.

4.4. Experiments with phantom B

Fig. 11 shows that the signal decay from experiments with phantom B follows a non-monoexponential behaviour typical of lung diffusion experiments, with slower decay rate at higher b-values. The experimental data fits Eq. (12), but it deviates from the theoretical behaviour obtained assuming $D_L = D_0$ and D_T calculated using Eq. (8) from the tubes known radius. The deviation of the signal decay from the monoexponential behaviour, though significant, is less than theoretically predicted by the original cylinder model. Fig. 11 also shows the theoretical signal behaviour predicted by the updated cylinder model (Eqs. (9)), which also deviates from the experimental data, although the deviation is smaller. Unlike the original model prediction, in this case the deviation from the experimental data is towards faster signal decay, as a result of the linear correction introduced in Eq. (9a), which produces an increase of D_T with increasing b-value.

Experimental data were fitted to both the original and the updated cylinder model, from which the estimates of the tube diameters were obtained (Table 3). The tube diameters were systematically over-estimated by the original cylinder model (Eqs. (12) and (8)), which again agrees with our previously published results [19] from computer simulations. When calculated using the updated cylinder model (Eqs. (12) and (9)), the tube diameters were systematically underestimated.

These discrepancies between the models and the experimental results may be due to superposition of competing effects of non-Gaussian signal behaviour in different parts of the phantom, with different orientations with respect to the gradients. The origin of these effects can be better understood by analyzing Fig. 9b. The solid lines in this figure represent the positions (in the diffusion dia-

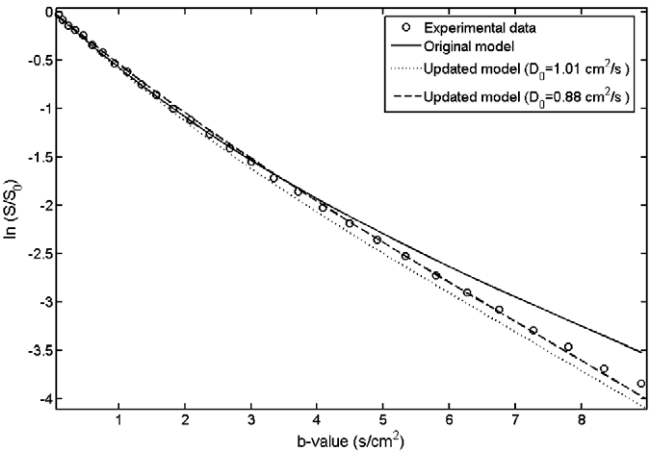

Fig. 11. Comparison of the theoretical signal behaviour and data obtained from the experiments with phantom B ($R = 1.02$ mm, $D_0 = 1.01$ cm^2/s). The theoretical behaviour predicted by the original model was obtained from Eq. (12), assuming $D_L = D_0$ and D_T as calculated using Eq. (8). Also shown are the theoretical behaviours predicted by the updated model of Eqs. (9) for $D_0 = 1.01$ cm^2/s and $D_0 = 0.88$ cm^2/s.

Table 3
Results of the diffusion experiments with phantom B ($D_0 = 1.01 \pm 0.02$ cm^2/s). The estimated tube diameters were calculated from the measured D_T using Eqs. (8) and (9).

Nominal tube diameter (±0.005 mm)	Estimated diameters (mm). Original model	Estimated diameters (mm). Updated model
0.760	0.79 ± 0.02	0.72 ± 0.02
1.020	1.12 ± 0.04	0.97 ± 0.03

gram) of the cylindrical elements (oriented in all angular directions) in phantom B. The measured signal for a given gradient strength then originates from elements that are in different diffusion regimes. For small gradients, most of the elements experience either free or restricted diffusion, where the Gaussian approximation is valid and Eqs. (3), (11) and (12) (and Eqs. (4) and (5) in 3D) should be valid. For large gradients, most of the elements are in the localization regime or its neighbouring intermediate regimes where the Gaussian approximation breaks down and Eqs. (3), (11) and (12) are no longer valid.

As shown in the previous section, depending on their angular position, tube volume elements can produce signals that can decay at either a rate faster (above ~40° in Fig. 9b) or slower rate (below ~40° in Fig. 9b) than a monoexponential for large gradients. The non-monoexponential behaviour of the bulk signal, is then not only due to the superposition of the signals originating from anisotropic diffusion in the individual tube elements, but also includes the competing effects of orientation-dependent non-Gaussian behaviour in the individual elements with different orientations, that have not bee taken into account by either model. The resulting signal behaviour would depend on which of these competing behaviours dominates, which would in turn be determined by a number of factors such as gas mixture, diffusion time and exact geometry and dimensions, as well as the actual angular distribution of airway orientations within each voxel (which in vivo may deviate from the assumed uniform distribution). This implies that there may be particular cases where these effects may balance each other and the cylinder model may hold. An example of this effect can be seen in Fig. 11 where the predicted theoretical behaviour for $D_0 = 0.88$ cm^2/s is shown. Even though this value of D_0 is 14% smaller than the experimentally determined D_0 value for this gas mixture, the calculated signal behaviour is a better fit of the experimental data than the theoretical signal calculated with the correct D_0.

This kind of result warrants further investigation, in particular, the sensitivity of the estimated diffusivities and airway dimensions to the free diffusion coefficient of the gas mixture since all reported works that use the cylinder model assume $D_0 = 0.88$ cm^2/s regardless of the exact gas mixture used. In a recently published study [34] that claims to validate the MR lung morphometry method (i.e. updated cylinder model) by comparison to histological measurements, even though the experiments were performed on excised and fixed lungs and the exact gas mixture composition was known, $D_0 = 0.88$ cm^2/s was still used. Although the actual D_0 was not measured, it is expected from theory [29] to be approximately 15% larger. Evaluating the results of such studies is hard, even more so for in vivo studies where knowledge of the gas composition and D_0 distribution in lung airways is not always available and the significance of this uncertainty for the results of the cylinder model has not yet been studied.

The results presented here demonstrate that the cylinder model (including the updates of [18]) is only valid if the localized diffusion regime and its neighbouring intermediate regimes are avoided. The intermediate regimes between localized diffusion and free diffusion and between localized diffusion and restricted diffusion are not well characterized and no simple analytical relationship between the signal behaviour and the geometry of the restricting structures exist. Experiments conducted in the localization regime become less sensitive to the exact geometrical shape and volume of the confining structures [13,15], instead being more sensitive to the surface area of the boundaries perpendicular to the diffusion gradient.

It is important to take this into account when designing PGSE ADC experiments since diffusion in acinar airways can fall into any one of these regimes or even into the intermediate regime where all three length scales are comparable and complex behaviour (e.g. diffraction-like patterns [15,32]) may occur.

Localized diffusion can be avoided by using weaker gradients (below ~15 mT/m for human lungs) and longer diffusion times. However, longer diffusion times would make branching effects (which are neglected in the cylinder model) more important and will decrease the achievable SNR by virtue of the incurred T_2^* decay in the delay time to signal acquisition. The use of weaker gradients may also make diffusion measurements more prone to the effects of background B_0 gradients.

Note that in this work only the basic physical assumptions of the cylinder model were tested in simple cylindrical phantoms. The cylinder model also includes other assumptions and approximations (e.g. effects of branching nodes and alveolar sac endings are neglected; effects of background susceptibility gradients are also ignored) whose limitations are yet to be investigated in detail. This investigation will be the subject of future work within the framework presented here.

5. Conclusions

In this work, the physical basis of the cylinder model has been tested experimentally in well defined cylindrical geometrical physical models of lung diffusion. Experiments and computer simulations have demonstrated that those physical assumptions are not valid for large diffusion gradient strengths (above ~15 mT/m), which are commonly used for ^{3}He ADC measurements in human lungs.

These results highlight the shortcomings of the cylinder model and other ADC-based approaches which are underpinned by the Gaussian phase approximation, which is only valid if the localization regime and its neighbouring intermediate regimes are avoided. If these regimes are not avoided, the complexity of the signal behaviour in those regimes should be considered and incorporated into subsequent models.

The updated cylinder model is a step in the right direction to include non-Gaussian diffusion effects in the model, but still relies on expressions founded on the Gaussian phase approximation. It does not account for angular dependent non-Gaussian effects and requires further development and validation.

When reporting results of ADC experiments it is important to include not only the *b*-values used. A complete description of the gradient sensitization waveform, including the timing parameters and gradient strength is required to correctly interpret these results and compare with results from other experiments.

The results obtained here and the simple phantoms and experimental procedures developed in this work may provide a framework to validate future models as well as help optimize the experimental design and interpret the results of lung MR experiments using hyperpolarized gases.

Acknowledgments

N. de Zanche (ETH Zurich) for help constructing the ^{3}He T–R switch. *Funding:* EU FP 6 Program Phelinet and EPSRC grant EPSRC # EP/D070252/1.

Appendix A

The diffusion signal originating from a collection of long cylinders uniformly distributed with orientations in all possible (2D) angular directions can be written as:

$$\frac{S(b)}{S_0} = \frac{\int_0^{\pi} \exp\left[-b(D_{\mathrm{L}}\ \cos^2\ \alpha + D_{\mathrm{T}}\ \sin^2\ \alpha)\right]\mathrm{d}\alpha}{\int_0^{\pi}\mathrm{d}\alpha}$$

$$\frac{S(b)}{S_0} = \frac{1}{\pi}\int_0^{\pi} \exp\left[-b(D_{\mathrm{L}}\ \cos^2\ \alpha + D_{\mathrm{T}}(1-\cos^2\ \alpha))\right]\mathrm{d}\alpha$$

$$\frac{S(b)}{S_0} = \frac{1}{\pi}\int_0^{\pi} \exp\left[-b(D_{\mathrm{AN}}\ \cos^2\ \alpha + D_{\mathrm{T}})\right]d\alpha$$

$$\frac{S(b)}{S_0} = \frac{1}{\pi}\exp\left[-bD_{\mathrm{T}}\right]\int_0^{\pi} \exp\left[-b(D_{\mathrm{AN}}\ \cos^2\ \alpha)\right]\mathrm{d}\alpha$$

$$\frac{S(b)}{S_0} = \frac{1}{\pi}\exp\left[-b\left(D_{\mathrm{T}} + \frac{D_{\mathrm{AN}}}{2}\right)\right]\int_0^{\pi} \exp\left[-\frac{bD_{\mathrm{AN}}}{2}\ \cos\ 2\alpha\right]\mathrm{d}\alpha$$

Defining $\bar{D}_{2\mathrm{D}} = D_{\mathrm{T}} + \frac{D_{\mathrm{AN}}}{2}$, after making the substitutions $u = 2\alpha$ and $x = \frac{bD_{\mathrm{AN}}}{2}$, the following expression is obtained:

$$\frac{S(b)}{S_0} = \frac{1}{2\pi}\exp\left[-b\bar{D}_{2\mathrm{D}}\right]\int_0^{2\pi} \exp[-x\ \cos\ u]\mathrm{d}u$$

The integral above is the integral representation of the modified Bessel function of the first kind, $I_0(x)$ [33]. The net behaviour of the diffusion signal in a cylindrical loop then results in the expression of Eq. (13):

$$\frac{S(b)}{S_0} = \exp\left[-b\bar{D}_{2\mathrm{D}}\right]I_0\left(\frac{bD_{\mathrm{AN}}}{2}\right).$$

References

[1] M. Salerno, T.A. Altes, J.P. Mugler, M. Nakatsu, H. Hatabu, E.E.. de Lange, Hyperpolarized noble gas MR imaging of the lung: Potential clinical applications, European Journal of Radiology 40 (2001) 33–44.

[2] H.E. Moller, X.J. Chen, B. Saam, K.D. Hagspiel, G.A. Johnson, T.A. Altes, E.E. de Lange, H.U. Kauczor, MRI of the lungs using hyperpolarized noble gases, Magnetic Resonance in Medicine 47 (2002) 1029–1051.

[3] M. Salerno, T.A. Altes, J.R. Brookeman, E.E. de Lange, J.P. Mugler, Rapid hyperpolarized ^{3}He diffusion MRI of healthy and emphysematous human lungs using an optimized interleaved-spiral pulse sequence, Journal of Magnetic Resonance Imaging 17 (2003) 581–588.

[4] M. Salerno, E.E. de Lange, T.A. Altes, J.D. Truwit, J.R. Brookeman, J.P. Mugler, Emphysema: hyperpolarized helium 3 diffusion MR imaging of the lungs compared with spirometric indexes – initial experience, Radiology 222 (2002) 252–260.

[5] A.J. Swift, J.M. Wild, S. Fichele, N. Woodhouse, S. Fleming, J. Waterhouse, R.A. Lawson, M.N.J. Paley, E.J.R. Van Beek, Emphysematous changes and normal variation in smokers and COPD patients using diffusion ^{3}He MRI, European Journal of Radiology 54 (2005) 352–358.

[6] J.C. Woods, C.K. Choong, D.A. Yablonskiy, J. Bentley, J. Wong, J.A. Pierce, J.D. Cooper, P.T. Macklem, M.S. Conradi, J.C. Hogg, Hyperpolarized ^{3}He diffusion MRI and histology in pulmonary emphysema, Magnetic Resonance in Medicine 56 (2006) 1293.

[7] D.A. Yablonskiy, A.L. Sukstanskii, J.C. Leawoods, D.S. Gierada, G.L. Bretthorst, S.S. Lefrak, J.D. Cooper, M.S. Conradi, Quantitative in vivo assessment of lung microstructure at the alveolar level with hyperpolarized ^{3}He diffusion MRI, Proceedings of the National Academy of Sciences of the United States of America 99 (2002) 3111–3116.

[8] B.T. Saam, D.A. Yablonskiy, V.D. Kodibagkar, J.C. Leawoods, D.S. Gierada, J.D. Cooper, S.S. Lefrak, M.S. Conradi, MR imaging of diffusion of He-3 gas in healthy and diseased lungs, Magnetic Resonance in Medicine 44 (2000) 174–179.

[9] R.E. Jacob, G. Laicher, K.R. Minar, 3D MRI of non-Gaussian ^{3}He gas diffusion in the rat lung, Journal of Magnetic Resonance 188 (2007) 357–366.

[10] S. Ajraoui, J. Parra-Robles, M. Deppe, K. Teh, S.R. Parnell, J. Owers-Bradley, J.M. Wild, Experimental investigation of non-gaussian diffusion in hyperpolarized ^{3}He MRI of lungs, Proceedings of the International Society for Magazine Resonance in Medicine 17 (2009) 2178.

[11] S. Fichele, M.N.J. Paley, N. Woodhouse, P.D. Griffiths, J.M. Wild, E.J.R. van Beek, Investigating ^{3}He diffusion NMR in the lungs using finite difference simulations and in vivo PGSE experiments, Journal of Magnetic Resonance 167 (2004) 1–11.

[12] C. Liu, R. Bammer, M.E. Moseley, Limitations of apparent diffusion coefficient-based models in characterizing non-Gaussian diffusion, Magnetic Resonance in Medicine 54 (2005) 419–428.

[13] M.E. Hayden, G. Archibald, K.M. Gilbert, C. Lei, Restricted diffusion within a single pore, Journal of Magnetic Resonance 169 (2004) 313–322.

[14] P.T. Callaghan, Principles of Nuclear Magnetic Resonance Microscopy, Oxford University Press, 1993.

[15] M.D. Hurlimann, K.G. Helmer, T.M.D. Swiet, P.N. Sen, C.H. Sotak, Spin echoes in a constant gradient and in the presence of simple restriction, Journal of Magnetic Resonance A 113 (1995) 260–264.

[16] P.T. Callaghan, K.W. Jolley, J. Lelievre, Diffusion of water in the endosperm tissue of wheat grains as studied by pulsed field gradient nuclear magnetic resonance, Biophysics Journal 28 (1979) 133–142.

[17] M. Paiva, Gaseous diffusion in an alveolar duct simulated by a digital computer, Computers and Biomedical Research 7 (1974) 533–543.

[18] A.L. Sukstanskii, D.A. Yablonskiy, In vivo lung morphometry with hyperpolarized ^{3}He diffusion MRI: Theoretical background, Journal of Magnetic Resonance 190 (2008) 200–210.

[19] S. Fichele, M.N.J. Paley, N. Woodhouse, P.D. Griffiths, E.J.R. van Beek, J.M. Wild, Finite-difference simulations of ^{3}He diffusion in 3D alveolar ducts: comparison with the "cylinder model", Magnetic Resonance in Medicine 52 (2004) 917–920.

[20] K. Emami, S. Kadlecek, S. Pickup, J.M. Woodburn, J. Zhu, J. Yu, V. Vahdat, M. Ishii, R. Cadman, S. Rajaei, T. Nakayama, C. Cox, R. Guyer, M. Law, M. Stephen, J. Shrager, D.A. Lipson, W. Gefter, R. Rizi, An improved technique for measurement of gas diffusion anisotropy in lung, Proceedings of the International Society for Magazine Resonance in Medicine 15 (2007) 2786.

[21] D. Habib, D.S. Grebenkov, X. Maitre, L.D. Rochefort, E. Durand, G. Guillot, Experimental study of gas diffusion in a pulmonary acinus model, Proceedings of the International Society for Magazine Resonance in Medicine 14 (2006) 1323.

[22] H. Kitaoka, S. Tamura, R. Takaki, A three-dimensional model of the human pulmonary acinus, Journal of Applied Physiology 88 (2000) 2260–2268.

[23] D.S. Grebenkov, G. Guillot, B. Sapoval, Restricted diffusion in a model acinar labyrinth by NMR: theoretical and numerical results, Journal of Magnetic Resonance 2007 (2007) 143–156.

[24] D.S. Grebenkov, G. Guillot, Localization regime of restricted diffusion in a model pulmonary acinus, Proceedings of the International Society for Magazine Resonance in Medicine 14 (2006) 1624.

[25] B. Saam, N. Drukker, W. Happer, Edge enhancement observed with hyperpolarized ^{3}He, Chemical Physics Letters 263 (1996) 481–487.

[26] T.M. de Swiet, Diffusive edge enhancement in imaging, Journal of Magnetic Resonance B 109 (1995) 12–18.

[27] C.H. Newman, Spin echo of spins diffusing in a bounded medium, Journal of Chemical Physics 60 (1974) 4508–4511.

[28] J. Parra-Robles, W.D. Viqueira, X. Xu, A. Ouriadov, G.E. Santyr, Theoretical prediction and experimental measurement of the field dependence of the apparent transverse relaxation of hyperpolarized noble gases in lungs, Journal of Magnetic Resonance 192 (2008) 85–91.

[29] R.H. Acosta, P. Blumler, L. Agulles-Pedros, A.E. Morbach, J. Schmiedeskamp, A. Herweling, U. Wolf, A. Scholz, W.G. Schreiber, W. Heil, M. Thelen, H.-W. Spiess, Controlling diffusion of ^{3}He by buffer gases: a structural contrast agent in lung MRI, Journal of Magnetic Resonance Imaging 24 (2006) 1291.

[30] T.A. Altes, J. Mata, E.E. de Lange, J.R. Brookeman, J.P. Mugler, Assessment of lung development using hyperpolarized helium-3 diffusion MR imaging, Journal of Magnetic Resonance Imaging 24 (2006) 1277.

[31] J.P. Mugler III, J.F. Mata, T.A. Altes, G.W. Miller, E.E. de Lange, W.A. Tobias, G.D. Cates Jr., J.R. Brookeman, Evidence of background-gradient effects in GRE-based ^{3}He diffusion MRI, Proceedings of the International Society for Magazine Resonance in Medicine 14 (2006) 1313.

[32] A. Coy, P.T. Callaghan, Pulsed gradient spin echo nuclear magnetic resonance for molecules diffusing between partially reflecting rectangular barriers, The Journal of Chemical Physics 101 (1994) 4599–4609.

[33] M. Abramowitz, I.A. Stegun, Handbook of Mathematical Functions: With Formulas, Graphs, and Mathematical Tables, Dover Publications, New York, 1972. p. 376.

[34] D.A. Yablonskiy, A.L. Sukstanskii, J.C. Woods, D.S. Gierada, J.D. Quirks, J.C. Hogg, J.D. Cooper, M.S. Conradi, Quantification of lung microstructure with hyperpolarized ^{3}He diffusion MRI, Journal of Applied Physiology 107 (2009) 1258–1265.